ELSEVIER

Journal of Structural Geology 25 (2003) 2035–2051

JOURNAL OF STRUCTURAL GEOLOGY

www.elsevier.com/locate/jsg

Quartz microstructures developed during non-steady state plastic flow at rapidly decaying stress and strain rate

Claudia A. Trepmann, Bernhard Stöckhert*

Institut für Geologie, Mineralogie und Geophysik, Ruhr-Universität Bochum, D-44780 Bochum, Germany

Received 9 July 2002; received in revised form 1 April 2003; accepted 4 April 2003

Abstract

Synseismic loading to very high stresses (>0.5 GPa) and subsequent creep during stress relaxation in the uppermost plastosphere at temperatures of ca. 300–350 °C, near the lower tip of an inferred once seismically active crustal scale fault, was proposed based on peculiar microstructures identified in rocks exposed over >100 km^2 in the Sesia Zone, European Western Alps. Here we discuss the conspicuous and highly heterogeneous microstructural record of quartz in disseminated small-scale shear zones. Sub-basal deformation lamellae and arrays of elongate subgrains on the TEM-scale indicate an early stage of glide-controlled deformation at high stresses. Distributed brittle failure is indicated by healed microcracks. Very fine-grained recrystallised aggregates with a pronounced crystallographic preferred orientation reflect intense plastic flow by dislocation creep. Locally, a fine-grained foam microstructure indicates a final stage of static grain growth at low differential stress. For the previously inferred peak stresses of about 0.5 GPa and given temperatures, initial strain rates on the order of 10^{-10} s^{-1} are predicted by available flow laws for dislocation creep of quartz. We emphasise the importance of short-term non-steady state deformation in the uppermost plastosphere underlying seismically active upper crust. The related heterogeneous record of quartz is governed by the local stress history at constant temperature.

Keywords: Quartz; Microfabric; Plasticity; Strain rate; Dislocation creep; Stress History

1. Introduction

Deformation of the brittle upper crust can be episodic, with a fault displacement on the order of metres taking place within seconds. The upper crustal layer within which earthquakes nucleate is termed the schizosphere, underlain by the plastosphere (Scholz, 1990). Note that this terminology is not just an equivalent to the conventional so-called crustal brittle-ductile transition, whose position is generally predicted based on extrapolation of an experimental flow law for quartz to a slow geological strain rate of 10^{-14} or 10^{-15} s^{-1} (e.g. Sibson, 1990). Instead, brittle deformation can propagate well into the plastosphere when loading is fast, or quasi-instantaneous, as expected for the stage of failure of the upper crust in major earthquakes. For such events, very high stresses and strain rates are predicted for the uppermost plastosphere. Clearly, an improved understanding of the response of the uppermost plastosphere to sudden displacement along faults during major earthquakes nucleating in the overlying schizosphere is essential for the appropriate evaluation of geodetic data recording postseismic creep (e.g. Pollitz et al., 2001; Vergnolle et al., 2001) and time dependent variations in the seismic properties of the crust (e.g. Baisch and Bokelmann, 2001). In this respect, reading the record of exhumed natural rocks, which is equivalent to a failure analysis in engineering science, provides unique insight into the mechanical response and conditions in the uppermost plastosphere that cannot be predicted from geophysical field experiments, simulations, or laboratory experiments.

Microstructural evidence for episodic deformation in the uppermost plastosphere related to failure of the schizosphere in major seismic events has been reported from the Sesia Zone, Western Alps (Küster and Stöckhert, 1999; Trepmann and Stöckhert, 2001, 2002). There, deformation at temperatures of about 300–350 °C beneath the lower tip of an inferred fault is characterised by extraordinarily high peak stresses exceeding 0.5 GPa, as indicated by the

* Corresponding author. Tel.: +49-234-3223227 or 3227254; fax: +49-234-3214572.

E-mail address: bernhard.stoeckhert@ruhr-uni-bochum.de (B. Stöckhert).

0191-8141/03/$ - see front matter © 2003 Elsevier Ltd. All rights reserved.
doi:10.1016/S0191-8141(03)00073-7

orientation distribution of mechanically twinned jadeite in metagranite (Trepmann and Stöckhert, 2001; Orzol et al., 2003), and supported by instantaneous fragmentation of the high-strength mineral garnet embedded in a quartz matrix (Trepmann and Stöckhert, 2002). The short-term deformation at very high stress is followed by creep during stress relaxation, which is suspected to be primarily controlled by the behaviour of quartz. The highly heterogeneous quartz microstructures in disseminated small-scale shear zones in micaschists and quartz veins, which are widespread in an area of >100 km^2, reveal a large variety of conspicuous and rather uncommon features. The results of an analysis of these quartz microstructures by optical microscopy, scanning (SEM) and transmission electron microscopy (TEM) are presented in this study, and discussed in terms of loading and relaxation history.

2. Geological setting, sampling, and analytical techniques

2.1. Geological setting

The Sesia Zone (Fig. 1) in the Western Alps is composed of continental crust derived from the basement of the southern overriding continent in the Alpine collision zone (Compagnoni et al., 1977). The rocks underwent an amphibolite or granulite facies metamorphism during the Variscan orogeny (Venturini, 1995). During Alpine subduction and collision they were buried to about 60 km depth and underwent an eclogite facies high pressure metamorphism at $T = 550 \pm 50$ °C and $P = 1.8 \pm 0.3$ GPa (Compagnoni, 1977; Pognante, 1989; Avigad, 1996) in the latest Cretaceous (Inger et al., 1996; Rubatto et al., 1999; Liermann et al., 2002). Eclogitic micaschists are the predominate rock type in the lower Aosta valley, composed of quartz, white mica, garnet, omphacite, epidote, some glaucophane, rutile, and apatite. K-feldspar and jadeite are important constituents of rocks with a granitic composition. For petrographic details the reader is referred to Compagnoni (1977) and Venturini (1995). The exhumation and cooling history of the Sesia Zone is constrained by fission track ages of zircon and apatite, which indicate cooling to below 280 ± 30 °C at ca. 35 Ma and below about 120 °C at ca. 25 Ma, respectively (Hurford et al., 1991). In the Oligocene and Miocene, the Sesia Zone was displaced upwards by several tens of kilometres with respect to the adjacent South Alpine basement (Ivrea Zone) along the Insubric Line, the western segment of the Periadriatic lineament (Schmid et al., 1989). In the lower Aosta valley, the structures and microstructures developed during high pressure metamorphism in the Cretaceous are overprinted by a late stage inhomogeneous ductile deformation (Richter, 1984) at temperatures of about 300–350 °C (Stöckhert et al., 1986). This stage of deformation, characterised by fluctuating pore fluid pressure, very high stress, and correspondingly high strain rates, took place during exhumation at a time when the rocks of the Sesia Zone constituted the uppermost plastosphere (Küster and Stöckhert, 1999; Trepmann and Stöckhert, 2001, 2002) and is addressed in the present study. Note that the precise position of the inferred fault in the overlying schizosphere is not known, as it did not propagate down into the presently exposed level and must have come to rest when the present day Sesia Zone became part of the brittle upper crust.

2.2. Sampling

The late stage plastic deformation is highly heterogeneous, with strain localised into millimetre- to decimetre-

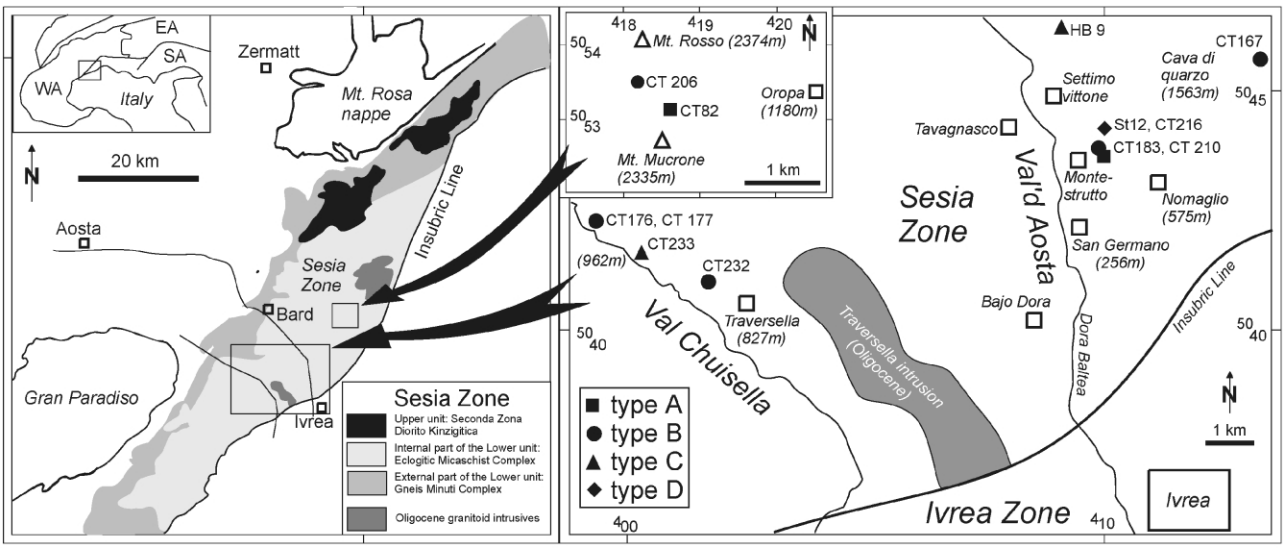

Fig. 1. Sketch map of the Sesia Zone and sample locations, with type of quartz microstructure visualised by symbols (A–D) and sample numbers (referred to in the text) indicated. EA = Eastern Alps, SA = Southern Alps, WA = Western Alps.

wide shear zones, with an extent that is generally too small to be displayed on a map. These disseminated shear zones, lacking an obvious uniform or systematic orientation pattern, are characterised by a prominent foliation and a weak to marked lineation. They are difficult to recognise in the field as the host rocks have undergone a complex previous deformation history (Richter, 1984). Outside these shear zones, the record of quartz is less specific due to limited strain, with intense plastic deformation and recrystallisation restricted to sites of stress concentration between rigid grains of other minerals. The location of the selected samples in the lower Aosta valley, Val Chuisella and at Mt. Mucrone is shown in Fig. 1, with the sample numbers and type of quartz microstructure, as referred to in this paper, indicated.

2.3. Analytical techniques

The rock samples were cut normal to the foliation and parallel to the lineation. The optical-scale quartz microstructures were examined in thin section with a polarising microscope. The orientation of the deformation lamellae and deformation bands was determined using a Leitz universal stage (U-stage) mounted on a Leitz Orthoplan microscope.

The crystallographic orientation and fine-scale microstructures of quartz were studied by scanning electron microscopy (SEM), using a LEO 1530 instrument with field emission gun, forescatter detector, and electron backscatter diffraction (EBSD) facilities. EBSD allows the determination of the full crystallographic orientation of crystals in a thin section using a backscattered electron (BSE) signal (e.g. Lloyd, 1987; Prior et al., 1996, 1999). It is complemented by orientation contrast (OC)-imaging, another SEM-based technique that visualises crystallographic misorientation between adjacent grains by greyscale contrast. Although this contrast does not correlate with the magnitude of misorientation, OC images provide information on the position and shape of grain boundaries. Automatic EBSD measurements were used to obtain orientation maps and crystallographic preferred orientation (CPO) patterns. In this case the sample was moved automatically in a grid-wise fashion underneath the focused electron beam and the crystallographic orientation was determined at each point. The EBSD patterns were indexed and orientation maps presented with the software 'CHANNEL 4' (Schmidt and Olesen, 1989). For presentation of CPO-patterns the program StereoNett 2.0 (Duyster, 1996) was used. All stereographic diagrams are lower hemisphere projections. The thin sections used for SEM-based techniques were chemically polished using a colloidal silicon suspension (SYTON®) to reduce the surface damage, and coated with carbon to prevent charging effects. The SEM was operated at an accelerating voltage of 25 kV, with the thin section tilted at an angle of 70° with respect to the beam, and with a working distance of 25 mm.

The arrangement and densities of dislocations and other submicroscopic features in quartz were analysed by transmission electron microscopy (TEM), using a Philips EM301 instrument operated at 100 kV, which requires thinning of the sample to less than about 200 nm. For preparation, polished thin sections were removed from the glass, broken into fragments, and thinned using a GATAN BIPS ion mill until small holes became visible. Observation in the TEM is restricted to the rims of these holes. All diffraction contrast images were produced using bright-field (BF) conditions.

The type and concentration of water and water-related defects in quartz were studied by Fourier-transform infrared microspectrometry (FTIR) (e.g. Kronenberg and Wolf, 1990), using an infrared (IR) spectrometer (Bruker IFS 48) with an attached IR-microscope. The IR microscope allows spectrometric analysis with a spatial resolution of ca. 0.1 mm, using polished sections of 0.1–0.2 mm thickness. FTIR measurements were performed both at room temperature (~295 K) and at a temperature of about 100 K in order to discriminate freezable water and to enhance the signal of point defects. The OH-concentration in quartz was calculated from the absorption spectra in the wave-number range of 3000–4000 cm^{-1} following the method proposed by Paterson (1982).

3. The microstructural record of quartz in the shear zones

According to the proportion of recrystallised grains, the quartz microstructures within the shear zones can be loosely grouped into four types, here referred to as types A to D. Type A microstructure is characterised by strong plastic deformation, but very limited recrystallisation, while type D microstructure is characterised by complete recrystallisation. Microstructures of the different types are found to occur adjacent to each other, showing no systematic distribution pattern in the investigated area (Fig. 1). In this paper, we first describe the overall characteristics of the type A to D microstructures. In the discussion we then deal with the significance of the individual microstructural features, their specific association, and the overprinting relationships.

3.1. Type A microstructure

Type A microstructures have been found at localities in the lower Aosta valley (sample CT183; coordinates 409.416E, 5043.518N, see Fig. 1) and at Mt. Mucrone (sample CT82; coordinates 418.486E, 5053.212N, see Fig. 1). For detailed analysis sample CT183 was chosen.

The type A quartz microstructure comprises barely recrystallised aggregates with a variable grain size of 10–100 μm and irregular shape (Fig. 2a–c). Sub-basal deformation lamellae (e.g. Avé Lallement and Carter, 1971), with the orientation identified by U-stage, are

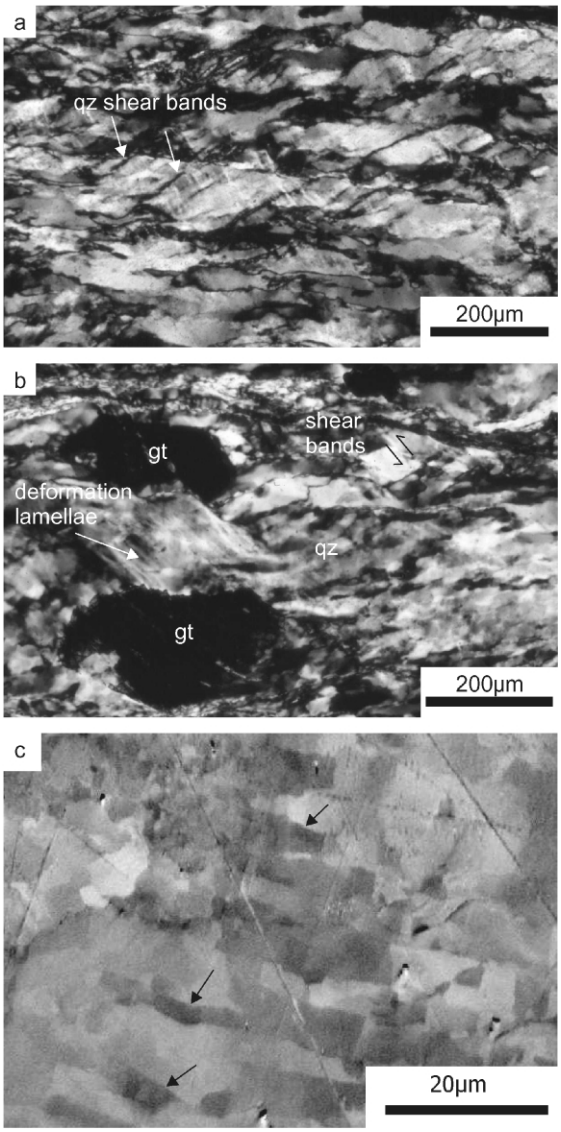

Fig. 2. Type A quartz microstructure (sample CT183, lower Aosta Valley). (a) Optical micrograph with crossed polars, showing deformation bands and shear bands with offset (arrows). (b) Optical micrograph taken with crossed polars, showing quartz deformation lamellae, which are parallel to shear bands with offset and to fractures in garnet. (c) OC-image of quartz microstructure with Dauphiné twins.

developed in some larger quartz crystals (Fig. 2b). Discrete shear bands with minor offset are common (Fig. 2a and b) and can be oriented parallel to deformation lamellae in quartz and fractures in garnet (Fig. 2b). Alternating dark and bright areas in OC-images (Fig. 2c) reveal the occurrence of Dauphiné twins, as confirmed by EBSD-measurements.

The highly heterogeneous type A quartz microstructure reveals a similarly heterogeneous submicroscopic structure in the TEM (Fig. 3), with curved dislocation walls or poorly ordered low-angle grain boundaries (Fig. 3a) defining elongate subgrains of irregular shape. Similar submicroscopic features are commonly associated with optical-scale deformation lamellae in naturally deformed quartz and in experimentally deformed metal alloys (Drury, 1993).

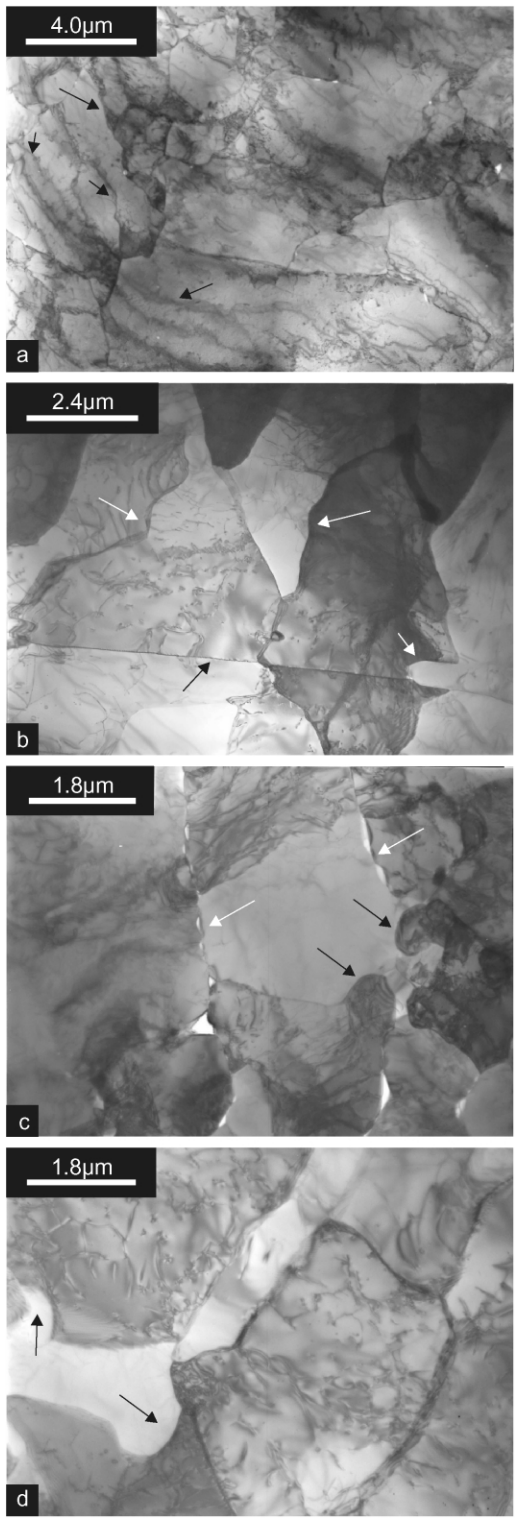

Fig. 3. TEM bright-field micrographs of the type A quartz microstructure (sample CT183, lower Aosta Valley). (a) Overview of inhomogeneous subgrain-structure and dislocation arrangement with curved irregular low angle grain boundaries bounding elongate subgrains (arrows). (b) Straight low-angle grain boundaries decorated with fluid inclusions (black arrow) and strongly curved grain boundaries (white arrows). (c) Parallel, straight grain boundaries decorated with fluid inclusions (white arrows) and bulging grain boundaries (black arrows). (d) Bulging grain boundaries (arrows).

Another conspicuous submicroscopic feature is the occurrence of straight low-angle grain boundaries, frequently decorated with fluid inclusions (Fig. 3b and c), which probably represent healed microcracks as they cut grain boundaries (Fig. 3b). Strongly curved, bulging high angle grain boundaries with a wavelength of about 0.5 μm (Fig. 3b–d) of larger quartz grains are indicative of strain-induced grain boundary migration. The free dislocation density varies within one order of magnitude between about 5×10^{13} m^{-2} and 2×10^{14} m^{-2}. In general, large grains reveal a higher free dislocation density compared with small recrystallised grains (Fig. 3d). Fluid inclusions of about 0.1–0.2 μm in diameter are mostly concentrated along grain boundaries, both low and high angles (Fig. 3a).

3.2. Type B microstructure

The type B microstructure appears to be the most widespread type, being found in five localities in the lower Aosta valley (sample CT210; coordinates 409.416E, 5043.518N; sample CT167; coordinates 413.114E, 5045.720N), in the Val Chuisella (samples CT176 and CT177; coordinates 398.877E, 5042.129N; sample CT232; coordinates 401.490E, 5040.885N) and at Mt. Mucrone (sample CT206; coordinates 418.354E, 5053.285N).

Characteristic for type B microstructures are quartz ribbons surrounded by recrystallised quartz grains (Fig. 4). The quartz ribbons measure up to 20 mm in length and 4 mm in width. The aspect ratio is variable, frequently exceeding a value of 10. The most conspicuous feature

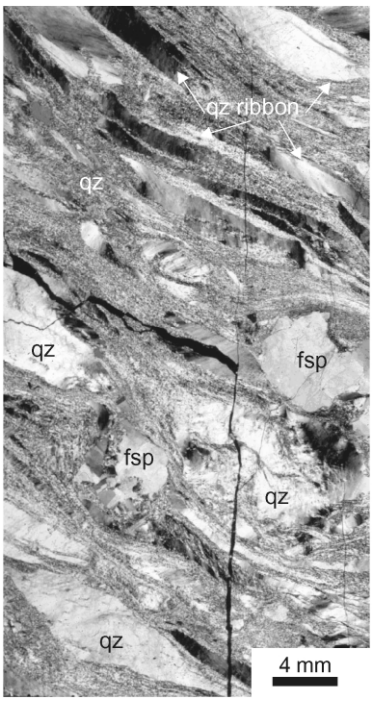

Fig. 4. Type B quartz microstructure (sample CT210, lower Aosta Valley) showing large quartz ribbons surrounded by recrystallised quartz grains and few feldspar porphyroclasts. Thin section scanned with crossed polars.

within these ribbons is deformation lamellae (Fig. 5a). They are visible in both plane-polarised light and with crossed polars as parallel to sub-parallel, closely-spaced planar or slightly undulating features, with an apparently slightly different refractive index or crystallographic orientation compared with the host grain. The spacing of the deformation lamellae is about 4.5 ± 2 μm. A sub-basal orientation, with an angle of about 10–30° to the basal plane was determined by U-stage. Sub-basal deformation lamellae conspicuous in the optical microscope are barely visible in OC-images (compare Fig. 6a and b). An EBSD-orientation map (Fig. 6c) of a quartz ribbon with deformation lamellae and the associated misorientation profile (Fig. 6d) reveal that the misorientation between the lamellae and the host grain is small, generally not exceeding 2°; this is close to the uncertainty of about 1° for EBSD-measurements (e.g. Lloyd, 1995). Deformation bands roughly parallel to the *c*-axis are discernible at a high angle to the sub-basal lamellae (Fig. 5a and b). Locally quartz ribbons resemble kinkbands (Fig. 5b).

In places, mutually parallel fluid inclusion trails transect the quartz ribbons at a high angle to their long axis, commonly revealing a small shear offset (Fig. 5c). These trails are interpreted to represent healed microcracks. Fig. 5d shows that these cracks can be restricted to a single subgrain within a quartz ribbon, where they are approximately parallel to the basal plane. This restriction indicates that brittle failure was controlled by the crystallographic orientation relative to the imposed stress field (e.g. Vollbrecht et al., 1999).

TEM investigation of sample CT177, characterised by the common occurrence of sub-basal deformation lamellae on the optical scale (Figs. 5a and 6a and b) reveals very small recrystallised grains, with a diameter down to <2 μm. The high angle grain boundaries are simply curved (Fig. 7a and c). These recrystallised grains appear to be nearly free of dislocations. Otherwise, most dislocations are geometrically necessary and arranged into well-ordered low-angle grain boundaries with tilt and twist geometry (Fig. 7c). The free dislocation density within larger grains is about 2 to 9×10^{12} m^{-2} (Fig. 7d). Only few subgrains (Fig. 7b) are elongate, as commonly observed in type A microstructures. Also, straight low-angle grain boundaries decorated with fluid inclusions, probably representing healed cracks, are only rarely observed (Fig. 7d). Some intragranular fluid inclusions occur in larger grains, where they are commonly associated with dislocations (Fig. 7d). Lens-shaped fluid inclusions decorate low and high angle grain boundaries (Fig. 7d).

The occurrence of well-ordered low-angle grain boundaries and small new grains nearly devoid of dislocations (Fig. 7a and c) are indicative of recovery and recrystallisation (e.g. White, 1977). Although deformation lamellae are conspicuous on the optical scale, submicroscopic features that could be unequivocally correlated with the lamellae are not identified by TEM.

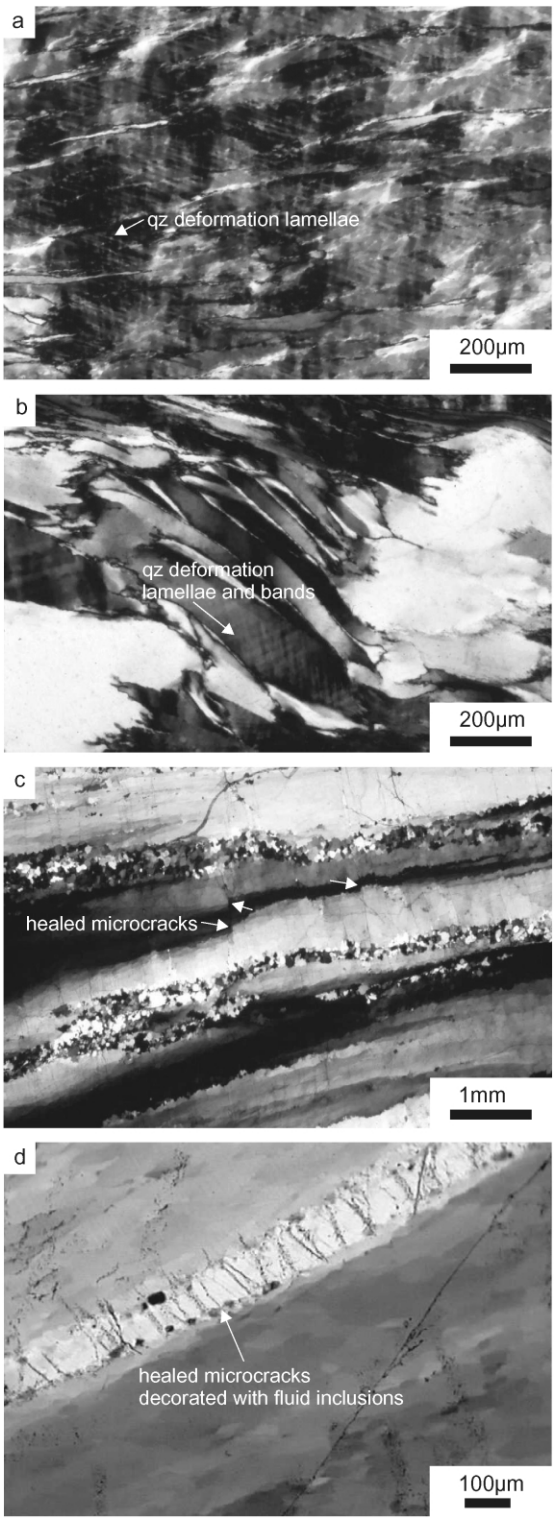

Fig. 5. Optical micrographs showing the type B quartz microstructure, all taken with crossed polars. (a) Microstructure showing extensive development of deformation lamellae in quartz crystals (sample CT177, Val Chuisella; micrograph taken with Red I compensator inserted). (b) Heterogeneous quartz microstructure with kink band-like, parallel quartz ribbons showing deformation lamellae and bands (sample CT176, Val Chuisella). (c) Parallel, healed microcracks with offset (sample CT232, Val Chuisella). (d) Parallel fluid inclusion trails restricted to a subgrain within a large quartz ribbo (sample CT210, lower Aosta Valley).

3.3. Type C microstructure

The type C microstructure is observed in samples from the Val Chuisella (sample CT233; coordinates 398.616E, 5042.385N) and from the lower Aosta valley (sample HB9; coordinates 409.100E, 5045.789N). Sample CT233 has been chosen for detailed investigation.

The type C quartz microstructure is highly heterogeneous, with aggregates of recrystallised grains with variable grain size (Fig. 8). The smallest observed grain size varies between 5 and 20 μm (Fig. 8d). Within larger grains, with a size between 20 and 50 μm, only very few deformation lamellae are discernible (Fig. 8b). The quartz grains are irregular in shape (Fig. 8a–d), with a marked shape preferred orientation (SPO), reflecting a heterogeneous strain field (Fig. 8a). Also, a distinct crystallographic preferred orientation (CPO) is developed (Fig. 9). The CPO reveals a point maximum of the *c*-axes perpendicular to the foliation plane and a maximum of the ⟨a⟩ axes in the foliation plane, indicating basal ⟨a⟩ glide.

Small-scale quartz veins perpendicular to the foliation (Fig. 8c) are obvious in the recrystallised quartz aggregates. The quartz crystals in these veins show subgrains and an identical or similar crystallographic orientation to adjacent grains in the matrix.

Most conspicuous at the submicroscopic scale in the TEM are elongate subgrains (Fig. 10a–c) with a width of approximately 0.5–1.6 μm and a length of about 4–7 μm. They show no specific orientation in a single sample (compare Fig. 10a–c). Recovery and recrystallisation are indicated by the arrangement of geometrically necessary dislocations in well-ordered low-angle grain boundaries (Fig. 10c) and by small (down to <2 μm) new-formed grains that are almost devoid of dislocations (Fig. 10d). Elsewhere, the free dislocation density is about 2 to 8×10^{12} m^{-2}.

3.4. Type D microstructure

Type D microstructures have been identified exclusively in the lower Aosta valley (sample St12; coordinates 409E, 5043N; sample CT 216; coordinates 409.555E, 5043.528N). Sample St12 was chosen for detailed investigation.

The type D quartz microstructure is a homogeneous fine-grained aggregate with a pronounced CPO. The grains are equant, with an average grain size of 7 μm. The grain boundaries are straight to simply curved (Fig. 11a–c). The CPO (Fig. 12) shows mostly a distinct point maximum of the ⟨c⟩ axes in the shortening (*Z*-) direction, while the maximum of the orientation of the ⟨a⟩ axes lies in the foliation (*XY*-) plane. This CPO implies basal slip in the ⟨a⟩ direction. Locally, the texture reveals a girdle of the ⟨c⟩ axes oriented about normal to the stretching (*X*-) lineation, suggesting that at these sites ⟨a⟩ slip on the rhombohedral and prism planes was activated as well. Similar to the type C microstructures, micrometer-wide quartz veins oriented

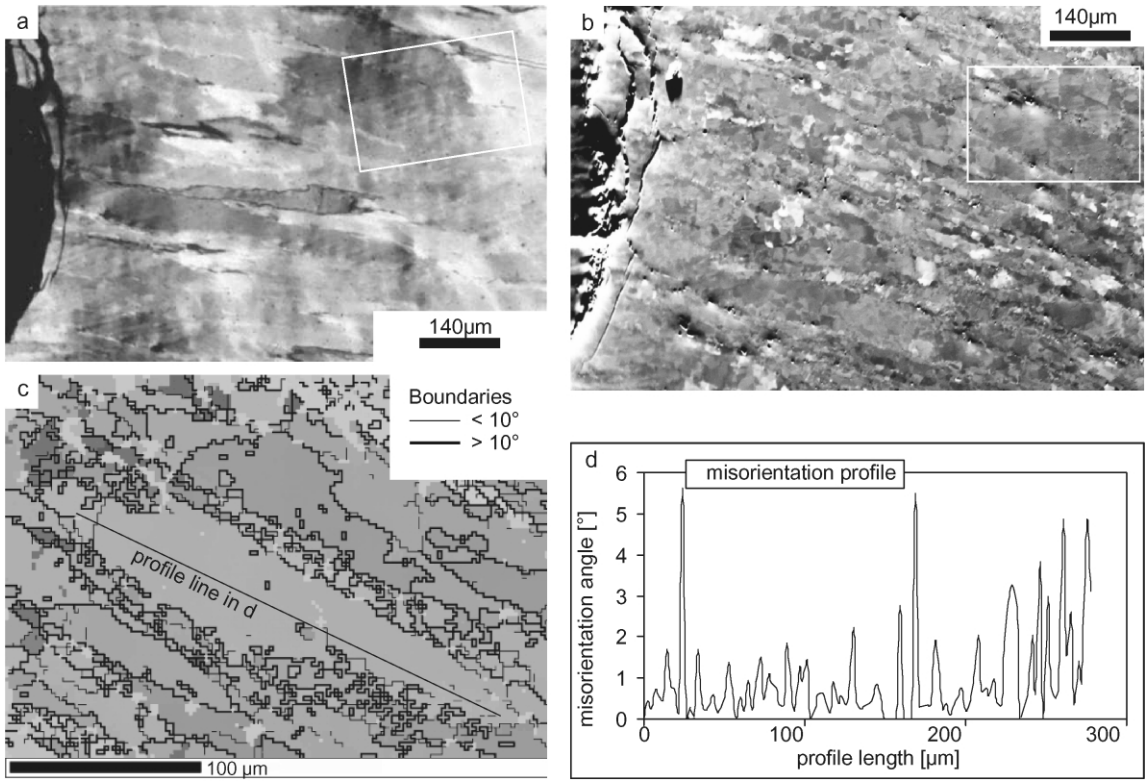

Fig. 6. (a) Optical micrograph of type B quartz microstructure, taken with crossed polars, showing quartz grains with sub-basal deformation lamellae (sample CT177, Val Chuisella); the white rectangle marks the position of the EBSD-map shown in (c). (b) OC-image of the region shown in (a). (c) EBSD-map of a region shown in (a) and (b) by a white rectangle and a profile line. Thick black lines mark high angle (>10°) and thin black lines mark low angle (2–10°) grain boundaries. (d) Misorientation profile recorded along the line marked in (c).

perpendicular to the foliation are observed in places (Fig. 11a).

On the TEM scale, the recrystallised grain size is found to be smaller than that discernible on the optical scale, with a typical grain diameter of about 2–5 µm. This discrepancy may be caused by the pronounced CPO, which masks certain grain boundaries due to vanishing contrast for respective positions of the rotating stage when viewed in the polarising microscope. Also, a typical foam structure with straight or simply curved grain boundaries meeting at near-120° angles at the grain edges (Fig. 13a) is conspicuous in the TEM. In other places, low-angle grain boundaries (Fig. 13b–d), which in part delineate strongly elongate subgrains (Fig. 13c), and dislocation tangles are observed. The free dislocation density is in the range of about 2 to 8×10^{12} m^{-2}. Fluid inclusions (Fig. 13c and d) occur along both low-angle and high-angle grain boundaries. Intragranular fluid inclusions were not observed.

3.5. Type and concentration of water and water-related defects

FTIR-microspectrometric analyses were performed on selected quartz samples with different microstructures to obtain information on the type and concentration of molecular water and water-related defects. At room temperature, the FTIR spectra reveal a broad absorption band extending from around 3700 cm^{-1}, through a maximum at about 3400 cm^{-1}, to around 3100 cm^{-1}. This broad absorption band represents aggregated molecular water (Paterson, 1989). In low-temperature spectra, recorded at about 100 K, a marked peak near 3200 cm^{-1} corresponds to the absorption band of ice (Paterson, 1989), indicating molecular water in freezable fluid inclusions. Water-related point defects that commonly appear as sharp peaks in the low-temperature FTIR-spectra are not discernible. The marked ice-band in the low-temperature FTIR-spectra indicates that molecular water in submicroscopic fluid inclusions is the dominant OH-species. The TEM images suggest that the fluid inclusions are concentrated along grain boundaries, with only a few occurring as intragranular fluid inclusions (Figs. 3c, 7d and 13d). The bulk water content of the quartz aggregates was calculated from the absorption spectra, measured at temperatures of about 100 K, using the method of Paterson (1982). The FTIR-spectra of completely recrystallised type D quartz aggregates indicate the highest water content with 2500–4000 ppm H/Si. The quartz grains from the type A and B microstructures showing deformation lamellae contain less than 2500 ppm H/Si. Barely deformed quartz grains of type B microstructures reveal the lowest water content of less than 1000 ppm H/Si.

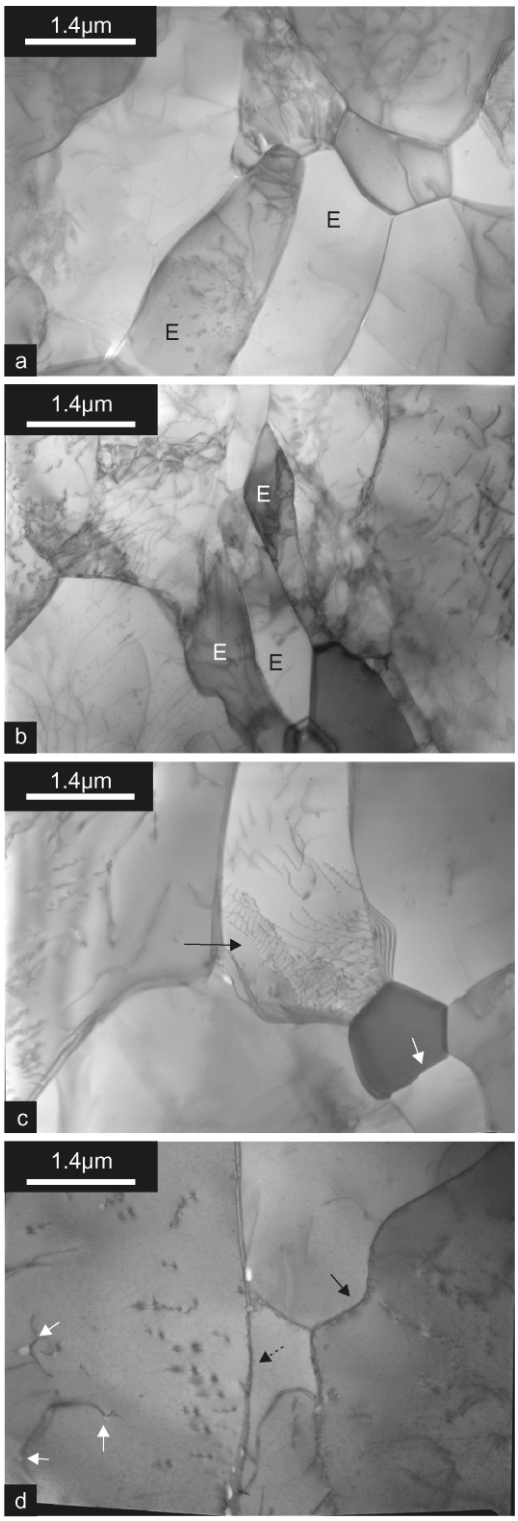

Fig. 7. TEM bright-field micrographs of type B quartz microstructure (sample CT177, Val Chuisella). (a) Elongate grains (E) with simply curved boundaries and low dislocation density. (b) Elongate subgrains (E). (c) Small dislocation-free grain with slightly curved boundaries (white arrow) and larger grain with a low angle grain boundary with twist geometry (black arrow). (d) Grain with a strongly curved grain boundary (black arrow) and a straight low angle grain boundary decorated with fluid inclusions (dashed arrow). Bent dislocations with dipoles pinned at fluid inclusions are marked by a white arrow.

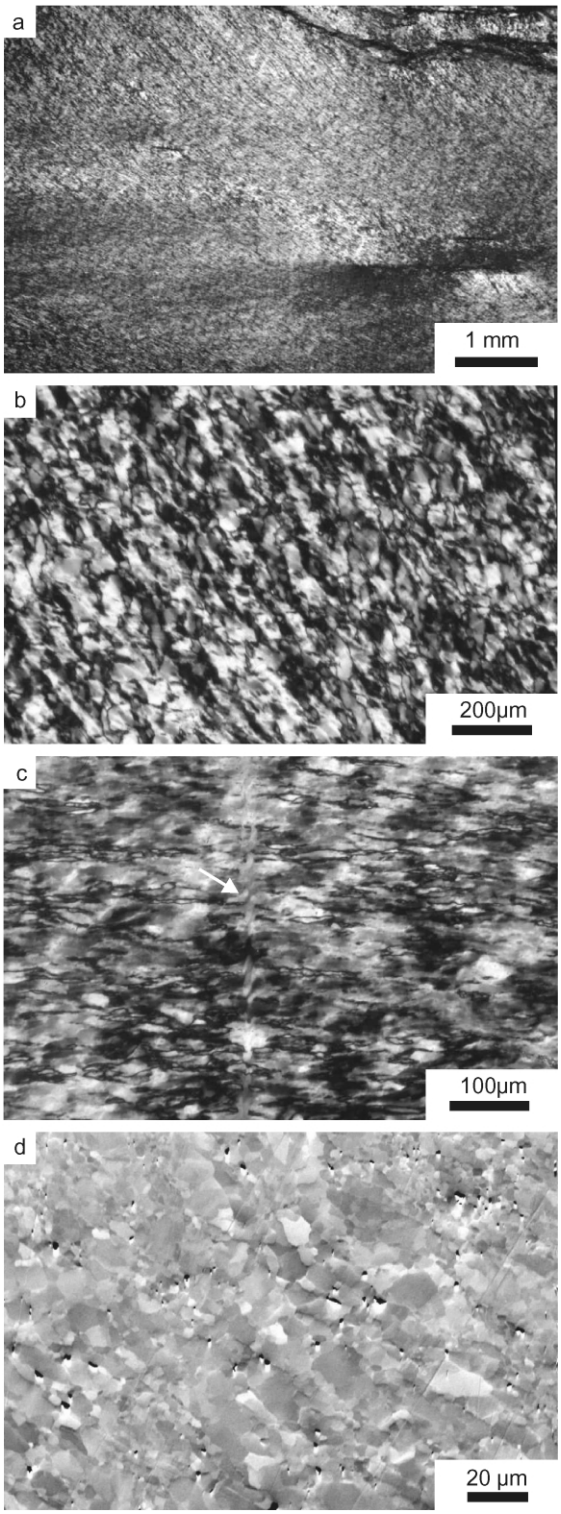

Fig. 8. Optical micrographs taken with crossed polars showing the type C quartz microstructure (sample CT233, Val Chuisella). (a) Microstructure with variable SPO around a calcite porphyroclast. (b) Recrystallised grains; a few deformation lamellae (arrow) are barely discernible. (c) Small-scale quartz vein (arrow) perpendicular to foliation in recrystallised quartz aggregate. (d) OC-image of recrystallised quartz aggregate showing an irregular (sub-)grain structure.

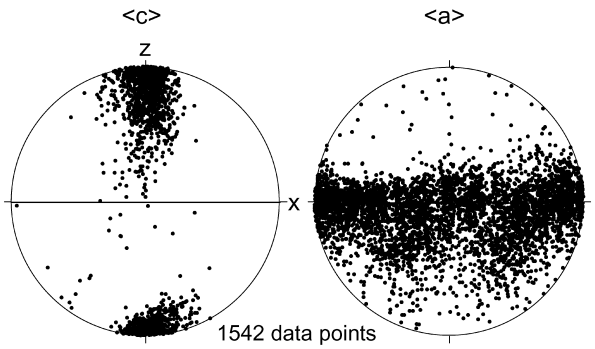

Fig. 9. Pole figures showing the orientation of quartz ⟨c⟩ and ⟨a⟩ axes of recrystallised grains in type C microstructure (sample CT233, Val Chuisella), determined by automatic EBSD-measurements. To minimise the effect of single crystal maxima a step width of 10 μm was chosen, which corresponds to the average grain size. The orientation of the ⟨c⟩ axes reveal a point maximum around the direction of shortening, and the ⟨a⟩ axes show a maximum within the foliation plane.

4. Discussion

The fact that microstructures preserved in natural deformed rocks compare well with those produced in laboratory experiments is generally taken to indicate identical deformation regimes (e.g. Hirth and Tullis, 1992, 1994; Hirth et al., 2001) and thus to allow extrapolation of experimental flow laws to natural conditions. However, this comparison must be performed very carefully, taking into account the cumulative strain and deformation history of natural rocks and the low preservation potential of certain microstructures during the prolonged natural thermal history in comparison to quenched laboratory samples. For instance, in the study by Stöckhert et al. (1999), successive overprinting of microstructures due to ongoing deformation during progressive cooling was related to temperature history. In contrast, in the present study, we emphasise the effect of short-term stress and strain rate variations at constant temperature. In the following, we first discuss the various microstructural indicators for the different deformation regimes passed by the samples, then some consequences for the application of paleopiezometers, and finally the overprinting relations and the preservation potential of the microstructures considering the inferred stress history.

4.1. Microstructures indicative of microcracking

Healed microcracks indicating a stage of brittle deformation of quartz are discernible in all types of microstructures. Some are decorated with fluid inclusions visible in the optical microscope (Fig. 5c and d). Küster and Stöckhert (1999) proposed that truncation of these planar arrays of fluid inclusions by mobile high angle grain boundaries can be taken as an indication of brittle failure at temperatures sufficient to allow subsequent deformation by dislocation creep. Experimental studies have shown that at these temperatures crack healing in quartz can be taken as

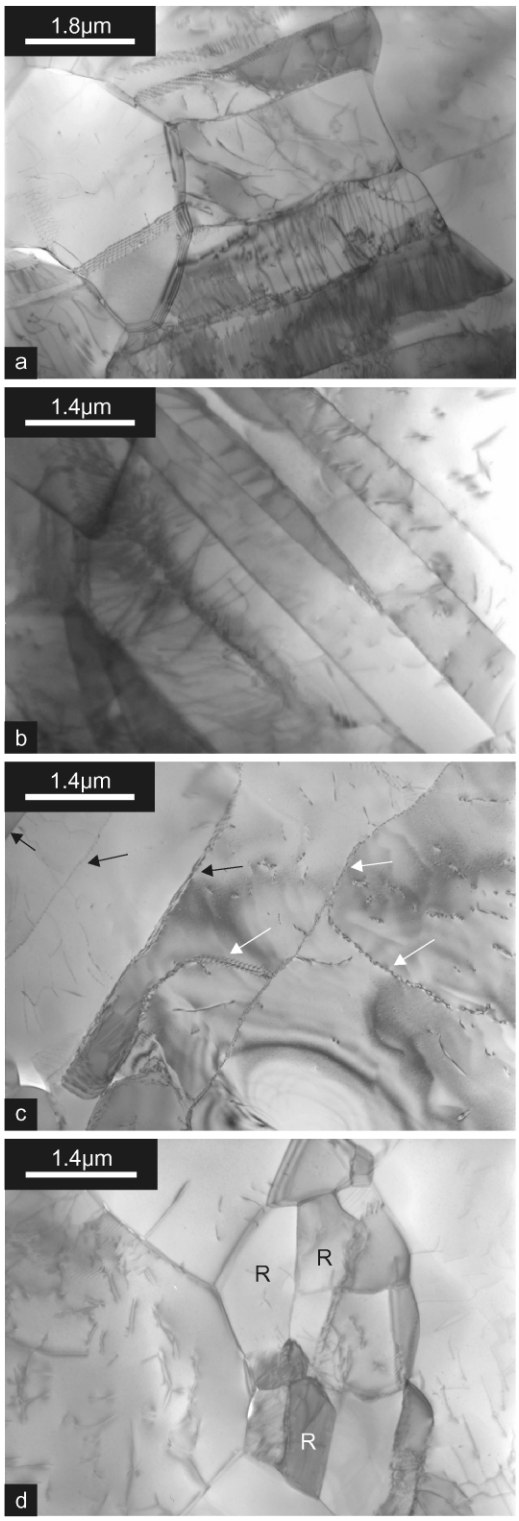

Fig. 10. TEM bright-field micrographs of recrystallised quartz aggregates of the type C microstructure (sample CT233, Val Chuisella). (a) Elongate subgrains with straight boundaries. (b) Straight parallel low angle grain boundaries bounding elongate subgrains with a width of less than 1 μm. (c) Straight parallel (black arrows) or simply curved low angle grain boundaries (white arrows). (d) Arrangement of small recrystallised grains (R).

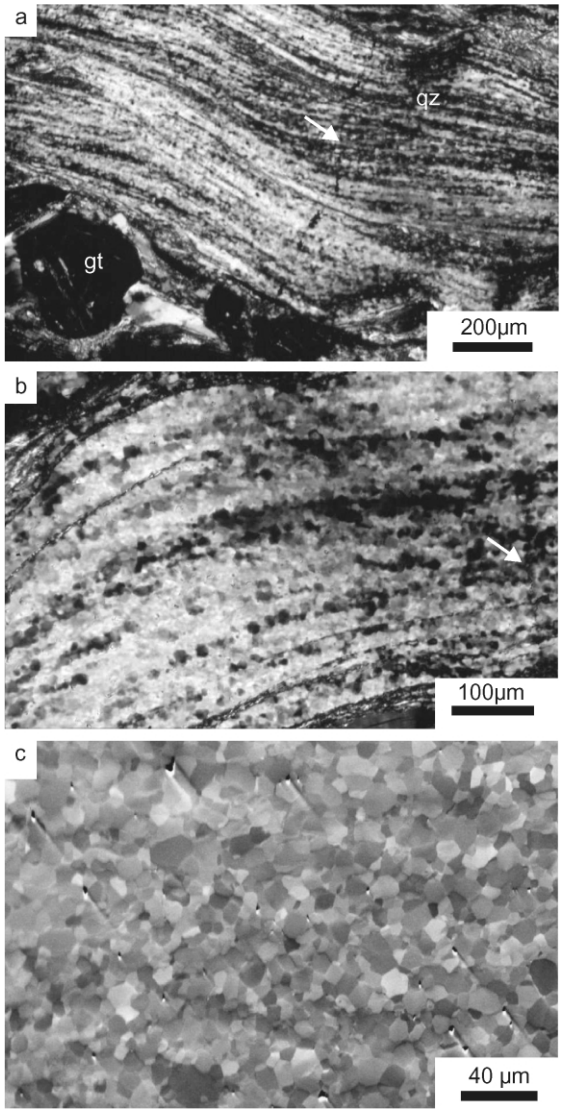

Fig. 11. Type D microstructure (sample St12, lower Aosta Valley). (a), (b) Optical micrographs (crossed polars) showing fine-grained recrystallised quartz aggregate with pronounced CPO; note small quartz vein perpendicular to the foliation (arrow) in (a). (c) OC-image showing quartz foam structure characterised by isometric grains with simply curved boundaries typically meeting at near-120° angles at the grain edges.

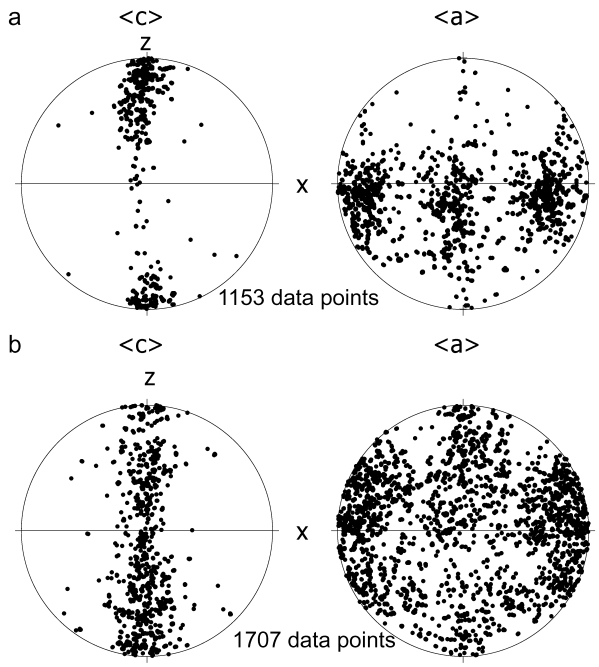

Fig. 12. CPO in type D microstructure (sample St 12, lower Aosta Valley). Quartz pole figures of ⟨c⟩ and ⟨a⟩ orientations, determined by automatic EBSD-measurements with a step width of 5 µm; the average grain size is about 7 µm. (a) The ⟨c⟩ axis orientations reveal a point maximum around the direction of shortening, and the ⟨a⟩ axis orientations a maximum within the foliation plane. (b) The orientation of the ⟨c⟩ axes shows a girdle maximum in the *YZ* plane. The ⟨a⟩ axes reveal an ill-defined point maximum around the *X* direction.

instantaneous on geological time scales (Smith and Evans, 1984). Furthermore, the planar low-angle grain boundaries decorated with fluid inclusions (Fig. 3b and c), which are observed by TEM in type A microstructures, may represent healed microcracks. The same holds true for discrete shear bands (Fig. 2a and b) with apparent offset in type A microstructures.

In contrast, evidence for microcracking in type C and D microstructures is largely restricted to the transgranular quartz-filled veinlets with a thickness of a few micrometers, mainly oriented perpendicular to the foliation in largely recrystallised quartz aggregates (Figs. 8c and 11a). The crosscutting relation and the fact that the quartz crystals grown in the vein have adopted the CPO of the matrix, indicate that the veinlets formed after significant deformation of the quartz matrix by dislocation creep. Notably, the vein quartz has also undergone minor deformation by dislocation creep. This indicates that the brittle failure leading to formation of these veinlets took place at a late stage of deformation, when an increased pore fluid pressure allowed the formation of dilatant cracks. Independent evidence for an increase of pore fluid pressure during progressive deformation, approaching a near-lithostatic value at a final stage of creep, comes from the opening of cracks in cataclastically deformed garnet in rocks with type C and D microstructures, as discussed by Trepmann and Stöckhert (2002).

The early-formed small scale microcracks, visible on the optical and in particular on the TEM scale in type A and B microstructures, were probably also formed in rocks now featuring type C and D microstructures, but have since been obliterated by subsequent recovery and recrystallisation. As such, type A and B microstructures, with limited recrystallisation, bear the record of an early stage of brittle deformation with a very high crack density, which was accompanied and followed by plastic flow. We propose that this stage of pervasive brittle failure is related to synseismic loading, with dilatancy and increased permeability causing the quasi-instantaneous drop of pore fluid pressure (Küster and Stöckhert, 1999), which is a prerequisite for crystal plastic flow at high differential stress.

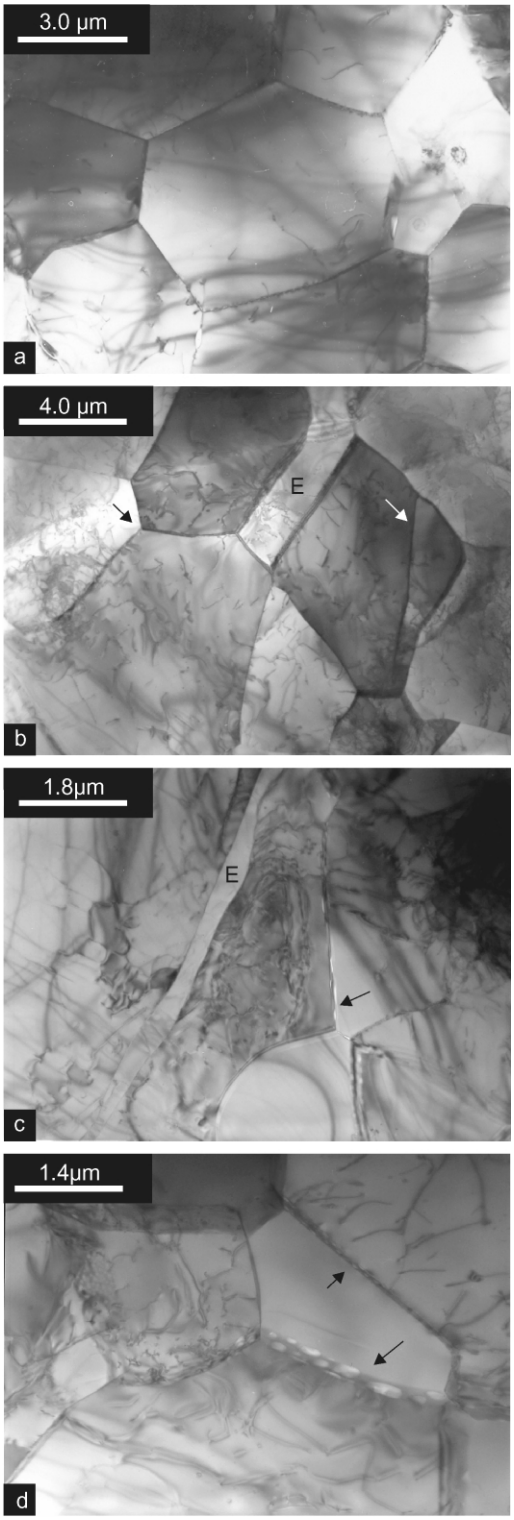

Fig. 13. TEM bright-field micrographs of recrystallised quartz aggregates in type D microstructure (sample St12, lower Aosta Valley). (a) Typical foam structure characterised by recrystallised grains with planar or simply curved boundaries making up near-120° angles at the grain edges. (b) Recrystallised grains with typical 120° angles between the grain boundaries at grain edges (black arrow), a low angle grain boundary (white arrow) and an elongate grain with straight, parallel boundaries (E). (c) Grain boundary decorated with fluid inclusions (arrow) and a very narrow, elongate subgrain (E). (d) Grain boundaries decorated with fluid inclusions (arrows).

4.2. Microstructures indicative of low-temperature plasticity

Notwithstanding the fact that the nature of sub-basal deformation lamellae, in particular on the TEM scale, remains a matter of debate (e.g. McLaren et al., 1970; McLaren and Hobbs, 1972; White, 1973, 1975; Christie and Ardell, 1974; Drury, 1993), Drury and Humphreys (1987) and Drury (1993) proposed that sub-basal deformation lamellae in quartz are indicative of glide-controlled deformation in the low-temperature plasticity field, being comparable with similar lamellae in metal alloys, which are only formed in that regime (McLaren and Hobbs, 1972; Drury and Humphreys, 1986, 1987; McLaren, 1991; Drury, 1993). Drury (1993) thus pointed out that the formation of deformation lamellae could possibly be taken as an indication for power law breakdown (e.g. Tsenn and Carter, 1987).

Previous TEM investigations have revealed that quite a number of different submicroscopic structures are associated with the optical-scale lamellae. In most cases the lamellae appear to be defined by arrays of elongate subgrains (McLaren and Hobbs, 1972; White, 1973; Blenkinsop and Drury, 1988; Drury, 1993), but can also be related to bands of variable dislocation density, or to planar arrays of fluid inclusions indicating microcracking (White, 1973, 1975; Christie and Ardell, 1974; White and Treagus, 1975; Drury, 1993). As their submicroscopic structure reveals substantial recovery (White, 1973; Christie and Ardell, 1974; Drury, 1993), sub-basal lamellae cannot be taken as unmodified discrete slip bands. Instead, Drury (1993) proposed that during glide-controlled deformation, geometrically necessary dislocations are generated in a certain plane, with those of like sign repelling each other after accumulation of some strain. The dislocations are then proposed to leave the original glide plane by cross slip or climb and to combine with dislocations from other glide planes. This process could eventually lead to an array of elongate subgrains.

In the small-scale shear zones investigated in this study, sub-basal deformation lamellae are most common in the type B microstructures (Figs. 5a and 6a). They are locally developed in the type A microstructures (Fig. 2b), and occasionally discernible in the type C microstructures (Fig. 8b). Regions with optically visible deformation lamellae in the type A microstructures show dislocation walls and poorly ordered low-angle grain boundaries on the TEM scale (Fig. 3a). Although deformation lamellae on the optical scale are even more prevalent in the type B microstructures, no obviously correlated microstructure is discernible on the TEM-scale. This indicates that recovery has obliterated the original TEM-scale structure of the deformation lamellae, leaving an array of elongate subgrains with well-ordered low-angle grain boundaries, and elongate recrystallised grains (Fig. 7a and b), both with a diameter of less than a few micrometers. Extremely

elongate subgrains are observed in type C microstructures (Fig. 10a–c), and locally even in type D microstructures (Fig. 13c). These TEM-scale microstructures are very similar to those described by McLaren and Hobbs (1972) from naturally deformed quartz from the Mt. Isa fault zone, north Queensland, Australia, who attributed these submicroscopic structures to non-steady state creep with strain hardening.

Notwithstanding the uncertain origin of deformation lamellae as slip bands or microcracks, the TEM-scale microstructures indicate extensive recovery after their formation, obliterating their original nature. On the scale accessible by the polarising microscope, however, they can still be discerned as arrays of planar features. If it is true that deformation lamellae are indicative of plastic deformation at high-stress (Drury, 1993), the present finding is consistent with the stress history inferred from independent evidence. Deformation lamellae have formed during short term plastic, and eventually brittle, deformation related to synseismic loading, and were subsequently modified by recovery, which was effective at the prevailing temperatures of 300–350 °C. This scenario could explain the wide variability of the reported submicroscopic structures related to deformation lamellae in natural quartz, which may in all cases indicate fluctuations in stress, with stages of short-term high stress plastic deformation, at temperatures sufficient for recovery. Such conditions may be typically met in the uppermost plastosphere near the lower tip of seismically active crustal scale faults. The ambient temperatures and the subsequent cooling history then determine the degree of recovery and obliteration of the original microstructures, and thus the wide variability of the TEM-scale features observed in quartz with deformation lamellae.

Rapid deformation of quartz in the low-temperature plasticity regime is expected to lead to strain hardening, with a very high strength reached after a few percent of strain (e.g. Hobbs, 1968). The corresponding high free dislocation densities are not observed in the present study, however, but have obviously been reduced to moderate values on the order of 10^{12} to 10^{13} m^{-2} during recovery. However, a very high original density of geometrically necessary dislocations, which are now arranged in low-angle grain boundaries, is indicated by the small subgrain size.

Dauphiné twins can originate as stress-induced deformation twins (Tullis, 1970; Barber and Wenk, 1991) and, based on recent studies using the EBSD/SEM technique, appear to be a common feature in quartz from naturally deformed rocks in a wide range of geological environments, from diagenetic to amphibolite facies conditions (e.g. Lloyd et al., 1992; Heidelbach et al., 2000; Lloyd, 2000; Neumann, 2000). As such, the Dauphiné twins—though probably stress-induced—are considered as unspecific microstructures, which do not provide further insight into the deformation history in the present context.

4.3. Microstructures indicative of recovery and recrystallisation

The arrangement of geometrically necessary dislocations into well-ordered low-angle grain boundaries, observed in all microstructural types (e.g. Figs. 3b, 7c and 10a–c), indicates effective recovery, leaving free dislocation densities on the order of 10^{12} to 10^{13} m^{-2}. Such dislocation densities correspond to the level commonly observed in quartz from metamorphic rocks (e.g. McLaren and Hobbs, 1972; White, 1976; Dresen et al., 1997; Stöckhert et al., 1999) and is well below that predicted for the high peak stresses in our study. Thus, the TEM-scale microstructure could principally be interpreted to result from recovery after early plastic deformation at high stress or to represent a late stage of creep after significant stress relaxation. Though a clear distinction is not feasible, we suppose that the small subgrain size reflecting an extraordinarily high concentration of geometrically necessary dislocations results from the early stage of glide-controlled deformation at very high differential stress. After formation by climb-controlled recovery in an early stage, the subgrains remained a stable microstructural feature, eventually becoming erased by recrystallisation during progressive deformation in type C and D microstructures. In contrast to the subgrains, the free dislocation density does not record the early deformation history.

Recrystallisation is commonly characterised as either rotation recrystallisation or migration recrystallisation (e.g. Guillopé and Poirier, 1979; Poirier, 1985). Also, recrystallisation that proceeds after or during deformation is referred to as static or dynamic, respectively (e.g. Nicolas and Poirier, 1976; Gottstein and Mecking, 1985; Urai et al., 1986). Obviously, both classifications may be not truly appropriate in the present context. Widespread evidence of migration recrystallisation is found on both optical and TEM-scale, where high-angle grain boundaries are sutured (Fig. 3c and d), or small grains appear to replace deformed larger grains in a core and mantle type structure (Fig. 5c). Initial rotation recrystallisation can be inferred from the pronounced CPO observed in type D microstructures (Fig. 12), with a continuous transition from subgrains bound by low-angle grain boundaries to recrystallised grains bound by high-angle grain boundaries. This transition results from the increase of misorientation due to geometrically necessary dislocations being progressively incorporated into the boundary. Grain boundary mobility depends on misorientation (e.g. Cotterill and Mould, 1976; Urai et al., 1986), rendering migration recrystallisation effective as soon as misorientation causes the boundary structure to change from an ordered dislocation wall into a disordered true high-angle grain boundary. For type C and D microstructures, we propose that subgrain formation graded into rotation recrystallisation, eventually followed by migration recrystallisation. In contrast, in the type A and B microstructures migration recrystallisation is observed to occur predomi-

nantly at pre-existing high angle grain boundaries, along small-scale shear bands, and at deformation lamellae. This indicates that in type A and B microstructures grain boundary migration is restricted to sites of pre-existing interfaces with a high degree of misorientation, or to sites of enhanced deformation due to local stress concentration.

Laboratory experiments have shown that quartz undergoes extreme strain hardening at high stress and strain rates (e.g. Hobbs, 1968). Transferred to the natural situation discussed here, this means that strain accumulated in the initial stage of glide-controlled deformation may be very limited. In contrast, the microstructures of the investigated shear zones indicate a considerable finite strain. Thus, the frozen microstructures observed on the optical and TEM scales are interpreted to reflect dynamic recovery and recrystallisation during progressive deformation by dislocation creep in the course of stress relaxation. This interpretation is supported by the similarity of the natural microstructures to those found in laboratory experiments on dislocation creep of quartz by Hirth and Tullis (1992). Type A microstructures correspond to those developed in dislocation creep regime 1, and the fine-grained type C and D recrystallised aggregates with pronounced CPO correspond to the dislocation creep regime 3 of Hirth and Tullis (1992). It should be noted, however, that the natural record does not reflect a steady state situation in terms of stress and strain rate.

Notwithstanding the overprint of the early microstructures by subsequent deformation in the dislocation creep regime, some characteristic features, such as the deformation lamellae discernible on the optical scale and the very small elongate subgrains visible by TEM, can be attributed to the early stage of high-stress deformation. These specific features are ubiquitous in the type A microstructure and largely or completely missing in the type D microstructure, indicating that they were erased by migration recrystallisation, in particular where high strain was accumulated in the stage of deformation by dislocation creep.

4.4. Crystallographic preferred orientation

The pronounced CPO associated with type C and D microstructures is related to the large amount of finite strain accumulated during deformation in the dislocation creep regime (e.g. Price, 1985). The CPO patterns reveal that basal ⟨a⟩ glide was the dominant slip system (Figs. 9 and 12), as expected for low to intermediate flow stress and greenschist-facies conditions (e.g. Hobbs, 1985; Schmid and Casey, 1986). In certain domains within type D microstructures, the CPO suggests that prism and rhombohedral ⟨a⟩ slip were also activated (Fig. 12), possibly due to local stress concentrations (Hobbs, 1985; Handy, 1990). In view of the highly inhomogeneous strain field on a larger scale, geometrical softening originating from the development of a pronounced CPO may have contributed to progressive localisation of deformation into the shear zones.

4.5. Microstructures indicative of grain growth

The type D microstructure reveals a characteristic foam structure on both the microscopic (Fig. 11c) and submicroscopic (Fig. 13a) scale. This foam structure is characterised by isometric grains with a diameter of a few micrometers, bound by planar or simply curved high angle grain boundaries meeting at near-120° angles along the grain edges, and a low free dislocation density. Such foam microstructures are indicative of static grain growth, driven by the reduction of interfacial free energy (e.g. Cotterill and Mould, 1976; Evans et al., 2001). Grain growth requires temperatures sufficient for grain boundary migration, and a very low differential stress precluding concomitant deformation by dislocation creep, as interfacial free energy is very low compared with elastic strain energy associated with an even moderate concentration of dislocations, and thus cannot control grain shape in materials undergoing deformation by dislocation creep. The observed foam structure is taken to indicate a final stage of annealing at very low differential stress, with temperatures still in the range of 350 ± 50 °C.

4.6. Paleopiezometers

The flow stress during steady state dislocation creep can be inferred from microstructural features (e.g. Poirier, 1985). Paleopiezometers based on recrystallised grain size, subgrain size, free dislocation density, and the spacing of deformation lamellae have been formulated and widely applied to natural rocks (e.g. Twiss, 1977, 1986; Ball and White, 1978; White, 1979; Christie and Ord, 1980; Kohlstedt and Weathers, 1980; Etheridge and Wilkie, 1981; Koch and Christie, 1981; Ord and Christie, 1984; Gleason and Tullis, 1993), assuming that the steady state microstructures are not significantly modified during the later geological history. Clearly, two of the basic prerequisites for the application of the above paleopiezometers are not met in the material investigated in the present study. First, deformation of quartz took place not by steady state dislocation creep, but was markedly non-steady state, and second, extensive modification of the original microstructures during annealing is indicated by the TEM-scale observations. As a consequence, application of the established paleopiezometers yields a very wide spectrum of inferred stresses, which are obviously all true for a certain—but not the same—stage of the deformation and relaxation history, with inferences on peak stress remaining as the only potentially valuable information.

4.7. Progressive evolution of the quartz microfabrics during postseismic stress relaxation

The initial stage of glide-controlled deformation in the low-temperature plasticity regime, indicated by the widespread deformation lamellae, associated with brittle failure,

indicated by healed microcracks, is proposed to be the result of synseismic loading (Fig. 14) during a large earthquake in the overlying schizosphere, as previously proposed by Küster and Stöckhert (1999) and Trepmann and Stöckhert (2001, 2002). During this stage, peak differential stresses of at least 0.5 GPa have been reached (Trepmann and Stöckhert, 2001). In view of the time scales inherent in the displacement along fault zones during earthquakes (e.g. Scholz, 1990), imposed strain rates may have exceeded those typically applied in laboratory experiments. Under similar conditions, plastic deformation of quartz in the laboratory is characterised by extensive strain hardening (e.g. Hobbs, 1968), leading to a transient strength of several GPa after accumulation of a few percent of strain.

After the earthquake, the displacement-induced stresses in the uppermost plastosphere are expected to decay, with the crust behaving as a Maxwell body (e.g. Ranalli, 1995) of unspecified length scale. The initial conditions during stress relaxation are provided by the peak stresses, which are limited by the ultimate strength of plastically deforming and hardening crust. The microstructures observed in the present study indicate that dislocation creep of quartz may be an important mechanism of stress relaxation. For the given temperatures of about 300–350 °C, and an initial stress of about 0.5 GPa, the power law $d\epsilon/dt = A\exp(-Q/RT)\sigma^n$ where the parameters $A = 6.5 \times 10^{-8}$ MPa^{-n}/s; $Q = 135 \pm 15$ kJ mol^{-1}; $n = 3.1$ experimentally derived by Paterson and Luan (1990) predicts strain rates on the order of 10^{-11} to 10^{-10} s^{-1}. It should be noted, however, that 0.5 GPa is about the stress level where the power law is expected to break down (e.g. Tsenn and Carter, 1987). Also, excess dislocation densities introduced during short-term plastic deformation need to be reduced by recovery before the predicted strain rates, based on a steady state microstructure, can be achieved. Depending on the rate of recovery, this may even lead to an initial increase of strain rate during stress relaxation. In the further course of stress relaxation the strain rates predicted by the power law decay rapidly, reaching the order of 10^{-13} s^{-1} at a stress level of about 0.1 GPa. Well-developed foam structures in some rocks indicate a final stage of interfacial free energy controlled grain growth at very low differential stress.

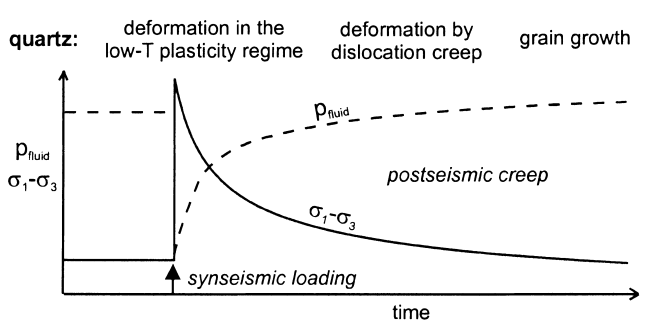

Fig. 14. Conceptual scheme visualising the inferred history of stress and pore fluid pressure during synseismic loading and postseismic creep in the uppermost plastosphere (after Trepmann and Stöckhert, 2002), and the respective deformation and resulting microstructural record of quartz, as documented and discussed in the present paper.

The microstructural record of quartz investigated in this study is extremely heterogeneous, but it is throughout consistent with the above scenario, implying instantaneous loading causing plastic and brittle deformation at very high stresses, followed by dislocation creep and finally low stress annealing. The heterogeneity is supposed to be partly due to small differences in temperature, which may amount to several tens of degrees Centigrade, simply related to paleodepth. However, there appears to be no systematic distribution of microstructural types within the investigated area, as revealed by the labelled sample locations in Fig. 1. This rules out temperature as the only reason of heterogeneity. Crustal inhomogeneity, with a wide variety of different rock types and pre-existing meso-scale structures can also cause a heterogeneous stress field on various length scales. As strain rate is highly sensitive to stress for power law creep, and even more so for low-temperature plasticity, even small stress gradients may cause significant strain gradients, and thus contrasts in the microstructural record. Also to be considered is that strain accumulated in the early stage of synseismic loading in the low-temperature plasticity regime may be limited by strain hardening, as indicated by the results of laboratory experiments on quartz (Hobbs, 1968). Localisation of deformation into shear zones then becomes pronounced during stress relaxation, when quartz is flowing in the dislocation creep regime, with progressive obliteration of the earlier record acquired in the low-temperature plasticity regime. The differences between the microstructural types A, B, C and D may roughly correlate with an increasing amount of strain accumulated in the dislocation creep regime.

Another factor relevant for the formation of the different microstructural types could be the relative importance of recovery versus recrystallisation. Given identical temperature and stress history, small differences in the availability of water could have influenced the mobility of high angle grain boundaries (e.g. Urai, 1983; Urai et al., 1986). Notably, the highest bulk water content of 2500–4000 ppm H/Si has been found by FTIR microspectrometry in sample St12 (type D microstructure), with a microstructural record indicating pronounced recrystallisation and final grain growth. The high angle grain boundaries are decorated with submicroscopic fluid inclusions. In contrast, the water content of quartz aggregates showing type A and B microstructures is mostly less than 1000 ppm H/Si, only exceptionally reaching 2500 ppm. A higher water content thus may cause recrystallisation to predominate over recovery, more effectively eliminating the high dislocation density introduced in the early stage of deformation in the low temperature plasticity regime compared with recovery, and thus facilitating flow in the dislocation creep stage.

Microcracking prior to or during plastic deformation might have increased the water content locally, consistent with healed microcracks decorated by fluid inclusions at the

optical microscopic (Fig. 5c and d) and TEM scale (Fig. 3b and c). Introduction of this water from an external source (e.g. Den Brok and Spiers, 1991) is indicated by the fact that the water content of quartz crystallised at high pressure metamorphism, and devoid of effects of the late stage deformation on the optical scale, is generally below the limit of detection, i.e. below 200 ppm H/Si (Meinecke, 1993). The water introduced in the early stage of distributed brittle failure and trapped in healed microcracks was possibly redistributed during subsequent deformation by dislocation creep, when the fluid inclusions were swept and drained by migrating high angle grain boundaries (Urai, 1983; Urai et al., 1986), with the fluid enhancing grain boundary mobility and thus making recrystallisation particularly effective.

In the present case study, the resulting quartz microstructures thus appear to be primarily controlled by (1) local stress history and (2) the relative rates of recovery and recrystallisation. The latter can be influenced by the availability of water, which was inhomogeneously introduced along cracks during the early stage of synseismic loading and then redistributed along migrating high angle grain boundaries (e.g. Urai, 1983; Urai et al., 1986) during the subsequent stage of dislocation creep. This concept contrasts with the commonly proposed correlation between the microstructural record of quartz and even small differences in temperature (e.g. Voll, 1976; Dunlap et al., 1997; Stöckhert et al., 1999; Hirth et al., 2001). Though the studied area provides a particularly conspicuous example, with very high peak stresses, the basic principle is considered to be valid in general. However, in many cases the record of loading and relaxation may be blurred by successive cycles superimposed upon each other, corresponding to the size–frequency distribution of earthquakes (e.g. Scholz, 1990) during progressive cooling. In the case of smaller earthquakes with short recurrence times compared with cooling history, the microstructural record of quartz may be dominated by the effect of temperature.

5. Conclusions

The peculiar stress history recorded by the rocks of the Sesia Zone, attributed to synseismic loading and postseismic creep in the uppermost plastosphere, with an extraordinarily high magnitude of peak stresses followed by stress relaxation and reconstitution of a near-lithostatic pore fluid pressure, as previously inferred from the microstructures of other minerals, is also reflected by the microstructural record of quartz. This record is governed by (1) short term deformation at very high stresses in the low-temperature plasticity field during synseismic loading, with limited finite strain due to strain hardening, followed by (2) dislocation creep at decreasing stresses and strain rates during stress relaxation, with dynamic recovery and recrystallisation, and finally (3) quasi static recovery and—after reduction of dislocation density to very low values—grain growth driven by interfacial free energy.

The microstructural record is the result of a sequence of processes that are superimposed on each other at nearly uniform temperature, but decaying differential stresses. Thus, flow was markedly non-steady state. At stage (1), strain rates may have even exceeded typical laboratory strain rates for a very short time, whereas dislocation creep at the given temperatures may have started, depending on the rate of recovery, with strain rates on the order of $10^{-10}\,s^{-1}$ for the indicated peak stresses. The strain rates then decayed during stress relaxation.

The conspicuous differences in the microstructural record of samples from different locations are attributed to small differences in temperature (as a function of paleodepth), in the initially accumulated plastic strain (e.g. as a function of position with respect to the inferred fault in the once overlying and meanwhile eroded paleo-schizosphere), and in the degree of strain localisation during stress relaxation (possibly depending on mesoscopic crustal inhomogeneity). Also, the relative importance of recovery and recrystallisation may be influenced by the non-uniform availability of water, enhancing grain boundary mobility.

In our case study, the microfabrics of quartz acquired in the brittle-plastic transition zone appear to be stress-controlled rather than simply a result of successive overprinting at decreasing temperature. Thus, they provide insight into the processes of short-term deformation of the uppermost plastosphere related to earthquakes, with information on peak stresses and stress history otherwise not accessible. Such results may be significant for the understanding of the earthquake cycle, for the inversion of related geodetic data, and for the modelling of syn- and postseismic deformation.

Acknowledgements

Many thanks are due to Klaus Röller for the instruction and help with the TEM. Rolf Neuser is thanked for support at the SEM, and Stuart Thomson for kindly improving the English. Funding by the German Science Foundation within the scope of the Collaborative Research Centre 526 “Rheology of the Earth—from the Upper Crust into the Subduction Zone” is gratefully acknowledged. A constructive review by Bas den Brok and critical questions posed by an anonymous referee are gratefully acknowledged.

References

Avé Lallement, H.G., Carter, N.L., 1971. Pressure dependence of quartz deformation lamellae orientations. American Journal of Science 270, 218–235.

Avigad, D., 1996. Pre-collisional ductile extension in the internal western

Alps (Sesia Zone, Italy). Earth and Planetary Science Letters 137, 175–188.

Baisch, S., Bokelmann, G.H.R., 2001. Seismic waveform attributes before and after the Loma Prieta earthquake: scattering change near the earthquake and temporal recovery. Journal of Geophysical Research 106, 16323–16337.

Ball, S., White, S., 1978. On the deformation of quartzite. Physical and Chemical Minerals 3, 163–172.

Barber, D.J., Wenk, H.R., 1991. Dauphiné twinning in deformed quartzites: implications of an in situ TEM study of the $\alpha-\beta$ phase transformation. Physical and Chemical Minerals 17, 492–502.

Blenkinsop, T.G., Drury, M.R., 1988. Stress estimates and fault history from quartz microstructures. Journal of Structural Geology 10, 673–684.

Christie, J.M., Ardell, A.J., 1974. Substructures of deformation lamellae in quartz. Geology 2, 405–408.

Christie, J.M., Ord, A., 1980. Flow stress from microstructures of mylonites: example and current assessment. Journal of Geophysical Research 85, 6253–6262.

Compagnoni, R., 1977. The Sesia-Lanzo Zone: high pressure-low temperature metamorphism in the Austroalpine continental margin. Rendiconti Societa Italiana della Mineralogia e Petrologia 33, 335–374.

Compagnoni, R., Dal Piaz, G.V., Hunziker, J.C., Gosso, G., Lombardo, B., Williams, P.F., 1977. The Sesia-Lanzo Zone, a slice of continental crust with alpine high pressure-low temperature assemblages in the western Italian Alps. Rendiconti Societa Italiana della Mineralogia e Petrologia 33, 281–334.

Cotterill, P., Mould, P.R., 1976. Recrystallization and Grain Growth in Metals, Surrey University Press, London.

Den Brok, S.W.J., Spiers, C.J., 1991. Experimental evidence for water weakening of quartzite by microcracking plus solution-precipitation creep. Journal of the Geological Society London 148, 541–548.

Dresen, G., Duyster, J., Stöckhert, B., Wirth, R., Zulauf, G., 1997. Quartz dislocation microstructure between 7000 m and 9100 m depth from the Continental Deep Drilling Program. KTB 102, pp. 18,443–18,452.

Drury, M.R., 1993. Deformation lamellae in metals and minerals. In: Boland, J.N., Fitzgerald, J.D. (Eds.), Defects and Processes in the Solid State: Geoscience Applications, The McLaren Volume, pp. 195–212.

Drury, M.R., Humphreys, F.J., 1986. The development of microstructures in Al-5% Mg during high temperature deformation. Acta Metallica 34, 2259–2271.

Drury, M.R., Humphreys, F.J., 1987. Deformation lamellae as indicator of stress level. EOS. Translations American Geophysical Union 44, 1471.

Dunlap, W.J., Hirth, G., Teyssier, C., 1997. Thermomechanical evolution of a ductile duplex. Tectonics 16, 983–1000.

Duyster, J., 1996. StereoNett 2.0. University of Bochum.

Etheridge, M.A., Wilkie, J.C., 1981. Grain size reduction, grain boundary sliding and the flow strength of mylonites. Tectonophysics 58, 159–178.

Evans, B., Renner, J., Hirth, G., 2001. A few remarks on the kinetics of static grain growth in rocks. International Journal of Earth Sciences 90, 88–103.

Gleason, G.C., Tullis, J., 1993. Improving flow laws and piezometers for quartz and feldspar aggregates. Geophysical Research Letters 20, 2111–2114.

Gottstein, G., Mecking, H., 1985. Recrystallization. In: Wenk, H.R., (Ed.), Preferred Orientation in Deformed Metals and Rocks—An Introduction to Modern Texture Analysis, Academic Press, New York, pp. 183–218.

Guillopé, M., Poirier, J.P., 1979. Dynamic recrystallization during creep of single-crystalline halite: an experimental study. Journal of Geophysical Research A 84, 5557–5567.

Handy, M.R., 1990. The solid state flow of polymineralic rocks. Journal of Geophysical Research 95, 8647–8662.

Heidelbach, F., Kunze, K., Wenk, H.R., 2000. Texture analysis of a recrystallised quartzite using electron diffraction in the scanning electron microscope. Journal of Structural Geology 22, 91–104.

Hirth, G., Tullis, J., 1992. Dislocation creep regimes in quartz aggregates. Journal of Structural Geology 14, 145–159.

Hirth, G., Tullis, J., 1994. The brittle-plastic transition in experimentally deformed quartz aggregates. Journal of Geophysical Research 99, 11731–11747.

Hirth, G., Teyssier, C., Dunlap, W.J., 2001. An evaluation of quartzite flow laws based on comparisons between experimentally and naturally deformed rocks. International Journal of Earth Science 90, 77–87.

Hobbs, B.E., 1968. Recrystallization of single crystals of quartz. Tectonophysics 6, 353–401.

Hobbs, B.E., 1985. The geological significance of microfabric analysis. In: Wenk, H.R., (Ed.), Preferred Orientation in Deformed Metals and Rocks: An Introduction to Modern Texture Analysis, Academic Press, New York, pp. 463–484.

Hurford, A.J., Hunziker, J.C., Stöckhert, B., 1991. Constraints on the late thermotectonic evolution of the Western Alps: evidence for episodic rapid uplift. Tectonics 10, 758–769.

Inger, S., Ramsbotham, W., Cliff, R.A., Rex, D.C., 1996. Metamorphic evolution of the Sesia-Lanzo-Zone, Western Alps: time constraints from multi-system geochronology. Contributions Mineralogy and Petrology 126, 152–168.

Koch, P.S., Christie, J.M., 1981. Spacing of deformation lamellae as a paleopiezometer. EOS Translations American Geophysical Union 62, 1030.

Kohlstedt, D.L., Weathers, M.S., 1980. Deformation-induced microstructures, paleopiezometers, and differential stresses in deeply eroded fault zones. Journal of Geophysical Research 85, 6269–6285.

Kronenberg, A.K., Wolf, G.H., 1990. Fourier transform infrared spectroscopy determinations of intragranular water content in quartz-bearing rocks: implications for hydrolytic weakening in the laboratory and within the earth. Tectonophysics 172, 255–271.

Küster, M., Stöckhert, B., 1999. High differential stress and sublithostatic pore fluid pressure in the ductile regime—microstructural evidence for short term postseismic creep in the Sesia Zone, Western Alps. Tectonophysics 303, 263–277.

Liermann, H.-P., Isachsen, C., Altenberger, U., Oberhänsli, R., 2002. Behaviour of zircon during high-pressure, low-temperature metamorphism: case study from the Internal Unit of the Sesia Zone (Western Italian Alps). European Journal of Mineralogy 14, 61–71.

Lloyd, G.E., 1987. Atomic number and crystallographic contrast images with the SEM: a review of backscattered electron techniques. Mineralogy Magazine 51, 3–19.

Lloyd, G.E., 1995. An appreciation of the SEM electron channelling technique for petrofabric and microstructural analysis of geological materials. In: Bunge, H.J., Siegesmund, S., Skrotzki, W., Weber, K. (Eds.), Textures of Geological Materials, DGM Informationsgesellschaft MbH, pp. 109–125.

Lloyd, G.E., 2000. Grain boundary contact effects during faulting of quartzite: an SEM/EBSD analysis. Journal of Structural Geology 22, 1675–1693.

Lloyd, G.E., Law, R.D., Mainprice, D., Wheeler, J., 1992. Microstructural and crystal fabric evolution during shear zone formation. Journal of Structural Geology 14, 1079–1100.

McLaren, A.C., 1991. Transmission Electron Microscopy of Minerals and Rocks, Cambridge University Press, New York.

McLaren, A.C., Hobbs, B.E., 1972. Transmission electron microscope investigation of some naturally deformed quartzites. In: Heard, H.C., Borg, I.Y., Carter, N.C., Raleigh, C.B. (Eds.), Flow and Fracture of Rocks. Geophysical Monograms 16, American Geophysical Union, pp. 55–66.

McLaren, A.C., Turner, R.G., Boland, J.N., 1970. Dislocation structure of the deformation lamellae in synthetic quart; a study by electron and optical microscopy. Controls in Mineralogy and Petrology 29, 101–115.

Meinecke, J., 1993. Spezifikation und Verteilung von Wasser in gesteinsbildendem Quarz in Beziehung zu Kristallisationsbedingungen,

Druck-, Temperatur- und Verformungsgeschichte. PhD thesis, University of Bochum.

Neumann, B., 2000. Texture development of recrystallised quartz polycrystals unravelled by orientation and misorientation characteristics. Journal of Structural Geology 22, 1695–1711.

Nicolas, A., Poirier, J.P., 1976. Crystalline Plasticity and Solid State Flow in Metamorphic Rocks, Wiley-Interscience.

Ord, A., Christie, J.M., 1984. Flow stresses from microstructures in mylonitic quartzites of the Moine Thrust zone, Assynt area, Scotland. Journal of Structural Geology 6, 639–654.

Orzol, J., Trepmann, C.A., Stöckhert, B., Shi, G., 2003. Critical shear stress for mechanical twinning of jadeite–an experimental study. Tectonophysics, accepted for publication.

Paterson, M.S., 1982. The determination of hydroxyl by infrared absorption in quartz, silicate glasses and similar materials. Bulletin of Mineralogy 105, 20–29.

Paterson, M.S., 1989. The interaction of water with quartz and its influence in dislocation flow—an overview. In: Karato, S.-I., Toriumi, M. (Eds.), Rheology of Solids and of the Earth, Oxford University Press, pp. 107–142.

Paterson, M.S., Luan, F.C., 1990. Quartzite rheology under geological conditions. In: Knipe, R.J., Rutter, E.H. (Eds.), Deformation Mechanisms, Rheology and Tectonics. Geological Society Special Publication, 54, pp. 299–307.

Pognante, U., 1989. Lawsonite, blueschist and eclogite formation in the southern Sesia Zone, western Alps, Italy. European Journal of Mineralogy 1, 89–104.

Poirier, J.-P., 1985. Creep of Crystals—High Temperature Deformation Processes in Metals, Ceramics and Minerals, Cambridge University Press, Cambridge.

Pollitz, F.F., Wicks, C., Thatcher, W., 2001. Mantle flow beneath a continental strike-slip fault: postseismic deformation after the 1999 Hector Mine earthquake. Science 293, 1814–1818.

Price, G.P., 1985. Preferred orientations in quartzites. In: Wenk, H.R., (Ed.), Preferred Orientation in Deformed Metals and Rocks—An Introduction to Modern Texture Analysis, Academic Press, New York, pp. 385–406.

Prior, D.J., Trimby, P.W., Weber, D.U., Dingley, D., 1996. Orientation contrast imaging of microstructures in rocks using forescatter detectors in the scanning electron microscope. Mineralogy Magazine 60, 859–869.

Prior, J.P., Bolyle, A.P., Brenker, F., Cheadle, M.C., Day, A., Lopez, G., Peruzzo, L., Potts, G.J., Reddy, S., Spiess, R., Timms, N.E., Trimby, P., Wheeler, J., Zetterström, L., 1999. The application of electron backscatter diffraction and orientation contrast imaging in the SEM to textural problems in rocks. American Mineralogy 84, 1741–1759.

Ranalli, G., 1995. Rheology of the Earth, 2nd ed, Chapman and Hall.

Richter, F., 1984. Deformation und Metamorphose in der alpinen SubduktionsZone: Die Sesia-Lanzo-Zone im unteren Val d'Aosta, Norditalien. Unpubl. Thesis University of Bonn.

Rubatto, D., Gebauer, D., Compagnoni, R., 1999. Dating of eclogite-facies zircons: the age of Alpine metamorphism in the Sesia-Lanzo Zone (Western Alps). Earth and Planetary Science Letters 167, 141–158.

Schmid, S., Casey, M., 1986. Complete fabric analysis of some commonly observed quartz c-axis patterns. Geophysical Union and Geophysical Monographs 36, 263–286.

Schmid, S.M., Aebli, H.R., Heller, F., Zingg, A., 1989. The role of the Periadriatic Line in the tectonic evolution of the Alps. In: Coward M.P., Dietrich D., Park R.G. (Eds.), Alpine Tectonics. Geological Society London, Special Publication 45, pp. 153–171.

Schmidt, N.H., Olesen, N., 1989. Computer-aided determination of crystal-lattice orientation from electron-channeling patterns in the SEM. Canadian Mineralogist 27, 15–22.

Scholz, C.H., 1990. The Mechanics of Earthquakes and Faulting, Cambridge University Press, Cambridge.

Sibson, R.H., 1990. Fluids in tectonically active regimes of the continental crust. Mineralogical Association of Canada 18, 93–132.

Smith, D.L., Evans, B., 1984. Diffusional crack healing in quartz. Journal of Geophysical Research 89, 4125–4135.

Stöckhert, B., Jäger, E., Voll, G., 1986. K–Ar age determinations on phengites from the internal part of the Sesia Zone, Western Alps, Italy. Contributions to Mineralogy and Petrology 92, 456–470.

Stöckhert, B., Brix, M.R., Kleinschrodt, R., Huford, A.J., Wirth, R., 1999. Thermochronometry and microstructures of quartz—a comparison with experimental flow laws and predictions on the temperature of the brittle-plastic-transition. Journal of Structural Geology 21, 351–369.

Trepmann, C.A., Stöckhert, B., 2001. Mechanical twinning of jadeite—an indication of synseismic loading beneath the brittle-ductile transition. International Journal of Earth Science 90, 4–13.

Trepmann, C.A., Stöckhert, B., 2002. Cataclastic deformation of garnet: a record of synseismic loading and postseismic creep. Journal of Structural Geology 24, 1845–1856.

Tsenn, M.-C., Carter, N.-L., 1987. Upper limits of power law creep of rocks. Tectonophysics. 136, 1–26.

Tullis, J., 1970. Quartz: preferred orientation in rocks produced by Dauphiné twinning. Science 168, 1342–1344.

Twiss, R.J., 1977. Theory and applicability of a recrystallised grain size paleopiezometer. Pageoph. 115, 227–244.

Twiss, R.J., 1986. Variable sensitivity piezometric equations for dislocation density and subgrain diameter and their relevance to olivine and quartz. American Geophysical Union, Geophysical Monograph 36, 247–261.

Urai, J.L., 1983. Water assisted dynamic recrystallization and weakening in polycrystalline bischofite. Tectonophysics 96, 125–157.

Urai, J., Means, W.D., Lister, G.S., 1986. Dynamic recrystallization of minerals. In: Hobbs, B.E., Heard, H.C. (Eds.), Mineral and Rock Deformation: Laboratory Studies. American Geophysical Union, Geophysical Monograph 36, pp. 161–200.

Venturini, G., 1995. Geology, geochemistry and geochronology of the inner central Sesia Zone, Western Alps—Italy. Mémoires de Géologie No. 25, Lausanne.

Vergnolle, M., Pollitz, F.F., Calais, E., 2001. GPS results in Mongolia, postseismic deformation and implications on curst/mantle viscosity in Central Asia. EOS Translations AGU 82(47), Fall Meeting Supplement, Abstract. G31A-0130, F267.

Voll, G., 1976. Recrystallization of quartz, biotite and feldspars from Erstfeld to the Leventina nappe, Swiss Alps, and its geological significance. Schweiz. mineral. petrogr. Mitt. 56, 641–647.

Vollbrecht, A., Stipp, M., Olesen, N.O., 1999. Crystallographic orientation of microcracks in quartz and inferred deformation processes: a study on gneisses from the German Continental Deep Drilling Project (KTB). Tectonophysics 303, 279–297.

White, S., 1973. Deformation lamellae in naturally deformed quartz. Nat. Phys. Sci. 245, 26–28.

White, S., 1975. The effects of polyphase deformation on the intracrystalline defect structures of quartz. II. Origin of the defect structures. N. Jb. Miner. Abh. 123, 237–252.

White, S.H., 1976. The role of dislocation processes during tectonic deformation with special reference to quartz. In: Strens, R.J., (Ed.), The Physics and Chemistry of Minerals and Rocks, pp. 75–91.

White, S., 1977. Geological significance of recovery and recrystallisation processes in quartz. Tectonophysics 39, 143–170.

White, S., 1979. Paleo-stress estimates in the Moine Thrust Zone, Eriboll, Scotland. Nature 280, 222–223.

White, S., Treagus, J.E., 1975. The effects of polyphase deformation on the intracrystalline defect structures of quartz. I. The defect structures. N. Jb. Miner. Abh. 123, 219–236.